Two-photon excitation in scattering media by spatiotemporally shaped beams and their application in optogenetic stimulation

Aurélien Bègue,[1] Eirini Papagiakoumou,[1] Ben Leshem,[2] Rossella Conti,[1] Leona Enke,[1] Dan Oron,[2] and Valentina Emiliani[1,*]

[1]*Wavefront-engineering Microscopy Group, Neurophysiology and New Microscopies Laboratory, Paris Descartes University, 45 rue des Saints-Pères 75270 Paris Cedex 06, France*
[2]*Department of physics of Complex Systems, Weizmann Institute of Science, Rehovot 76100, Israel*
[*]*valentina.emiliani@parisdescartes.fr*

Abstract: The use of wavefront shaping to generate extended optical excitation patterns which are confined to a predetermined volume has become commonplace on various microscopy applications. For multiphoton excitation, three-dimensional confinement can be achieved by combining the technique of temporal focusing of ultra-short pulses with different approaches for lateral light shaping, including computer generated holography or generalized phase contrast. Here we present a theoretical and experimental study on the effect of scattering on the propagation of holographic beams with and without temporal focusing. Results from fixed and acute cortical slices show that temporally focused spatial patterns are extremely robust against the effects of scattering and this permits their three-dimensionally confined excitation for depths more than 500 μm. Finally we prove the efficiency of using temporally focused holographic beams in two-photon stimulation of neurons expressing the red-shifted optogenetic channel C1V1.

References and links

1. M. Reicherter, T. Haist, E. U. Wagemann, and H. J. Tiziani, "Optical particle trapping with computer-generated holograms written on a liquid-crystal display," Opt. Lett. **24**(9), 608–610 (1999).
2. C. Lutz, T. S. Otis, V. DeSars, S. Charpak, D. A. DiGregorio, and V. Emiliani, "Holographic photolysis of caged neurotransmitters," Nat. Methods **5**(9), 821–827 (2008).
3. P. Wang and R. Menon, "Three-dimensional Lithography via Digital Holography," in *Frontiers in Optics 2012/Laser Science XXVIII* (Optical Society of America, 2012), p. FTu3A.4.
4. J. E. Curtis, B. A. Koss, and D. G. Grier, "Dynamic holographic optical tweezers," Opt. Commun. **207**(1-6), 169–175 (2002).
5. R. W. Gerchberg and W. O. Saxton, "A pratical algorithm for the determination of the phase from image and diffraction pictures," Optik **35**, 237–246 (1972).
6. F. Wyrowski and O. Bryngdahl, "Speckle-free reconstruction in digital holography," J. Opt. Soc. Am. A **6**(8), 1171 (1989).
7. V. Nikolenko, K. E. Poskanzer, and R. Yuste, "Two-photon photostimulation and imaging of neural circuits," Nat. Methods **4**(11), 943–950 (2007).
8. S. Yang, E. Papagiakoumou, M. Guillon, V. de Sars, C. M. Tang, and V. Emiliani, "Three-dimensional holographic photostimulation of the dendritic arbor," J. Neural Eng. **8**(4), 046002 (2011).
9. F. Anselmi, C. Ventalon, A. Bègue, D. Ogden, and V. Emiliani, "Three-dimensional imaging and photostimulation by remote-focusing and holographic light patterning," Proc. Natl. Acad. Sci. U.S.A. **108**(49), 19504–19509 (2011).
10. M. A. Go, C. Stricker, S. Redman, H.-A. Bachor, and V. R. Daria, "Simultaneous multi-site two-photon photostimulation in three dimensions," J. Biophotonics **5**(10), 745–753 (2012).
11. E. Papagiakoumou, V. de Sars, D. Oron, and V. Emiliani, "Patterned two-photon illumination by spatiotemporal shaping of ultrashort pulses," Opt. Express **16**(26), 22039–22047 (2008).
12. E. Papagiakoumou, V. de Sars, V. Emiliani, and D. Oron, "Temporal focusing with spatially modulated excitation," Opt. Express **17**(7), 5391–5401 (2009).

13. I. M. Vellekoop and A. P. Mosk, "Focusing coherent light through opaque strongly scattering media," Opt. Lett. **32**(16), 2309–2311 (2007).
14. I. M. Vellekoop, A. Lagendijk, and A. P. Mosk, "Exploiting disorder for perfect focusing," Nature Photon. **4**(5), 320–322 (2010).
15. N. Ji, D. E. Milkie, and E. Betzig, "Adaptive optics via pupil segmentation for high-resolution imaging in biological tissues," Nat. Methods **7**(2), 141–147 (2010).
16. O. Katz, E. Small, Y. Bromberg, and Y. Silberberg, "Focusing and compression of ultrashort pulses through scattering media," Nature Photon. **5**(6), 372–377 (2011).
17. K. D. Wulff, D. G. Cole, R. L. Clark, R. Dileonardo, J. Leach, J. Cooper, G. Gibson, and M. J. Padgett, "Aberration correction in holographic optical tweezers," Opt. Express **14**(9), 4170–4175 (2006).
18. A. Jesacher, A. Schwaighofer, S. Fürhapter, C. Maurer, S. Bernet, and M. Ritsch-Marte, "Wavefront correction of spatial light modulators using an optical vortex image," Opt. Express **15**(9), 5801–5808 (2007).
19. T. Čižmár, M. Mazilu, and K. Dholakia, "In situ wavefront correction and its application to micromanipulation," Nature Photon. **4**(6), 388–394 (2010).
20. Z. Bouchal, J. Wagner, and M. Chlup, "Self-reconstruction of a distorted nondiffracting beam," Opt. Commun. **151**(4-6), 207–211 (1998).
21. V. Garcés-Chávez, D. McGloin, H. Melville, W. Sibbett, and K. Dholakia, "Simultaneous micromanipulation in multiple planes using a self-reconstructing light beam," Nature **419**(6903), 145–147 (2002).
22. F. O. Fahrbach, P. Simon, and A. Rohrbach, "Microscopy with self-reconstructing beams," Nature Photon. **4**(11), 780–785 (2010).
23. J. Glückstad and D. Palima, *Generalized Phase Contrast: Applications in Optics and Photonics* (Springer, 2009).
24. E. Papagiakoumou, F. Anselmi, A. Bègue, V. de Sars, J. Glückstad, E. Y. Isacoff, and V. Emiliani, "Scanless two-photon excitation of channelrhodopsin-2," Nat. Methods **7**(10), 848–854 (2010).
25. E. Papagiakoumou, A. Bègue, B. Leshem, O. Schwartz, B. M. Stell, J. Bradley, D. Oron, and V. Emiliani, "Functional patterned multiphoton excitation deep inside scattering tissue," Nature Photon. **7**(4), 274–278 (2013).
26. H. Dana, N. Kruger, A. Ellman, and S. Shoham, "Line temporal focusing characteristics in transparent and scattering media," Opt. Express **21**(5), 5677–5687 (2013).
27. O. Yizhar, L. E. Fenno, M. Prigge, F. Schneider, T. J. Davidson, D. J. O'Shea, V. S. Sohal, I. Goshen, J. Finkelstein, J. T. Paz, K. Stehfest, R. Fudim, C. Ramakrishnan, J. R. Huguenard, P. Hegemann, and K. Deisseroth, "Neocortical excitation/inhibition balance in information processing and social dysfunction," Nature **477**(7363), 171–178 (2011).
28. E. Y. S. Yew, H. Choi, D. Kim, and P. T. C. So, "Wide-field two-photon microscopy with temporal focusing and HiLo background rejection," Proc. SPIE **7903**, 79031O (2011).
29. H. Choi, E. Y. S. Yew, B. Hallacoglu, S. Fantini, C. J. R. Sheppard, and P. T. C. So, "Improvement of axial resolution and contrast in temporally focused widefield two-photon microscopy with structured light illumination," Biomed. Opt. Express **4**(7), 995–1005 (2013).
30. S. Gasparini, M. Migliore, and J. C. Magee, "On the initiation and propagation of dendritic spikes in CA1 pyramidal neurons," J. Neurosci. **24**(49), 11046–11056 (2004).
31. M. Oheim, E. Beaurepaire, E. Chaigneau, J. Mertz, and S. Charpak, "Two-photon microscopy in brain tissue: parameters influencing the imaging depth," J. Neurosci. Methods **111**(1), 29–37 (2001).
32. E. Chaigneau, A. J. Wright, S. P. Poland, J. M. Girkin, and R. A. Silver, "Impact of wavefront distortion and scattering on 2-photon microscopy in mammalian brain tissue," Opt. Express **19**(23), 22755–22774 (2011).
33. R. Prakash, O. Yizhar, B. Grewe, C. Ramakrishnan, N. Wang, I. Goshen, A. M. Packer, D. S. Peterka, R. Yuste, M. J. Schnitzer, and K. Deisseroth, "Two-photon optogenetic toolbox for fast inhibition, excitation and bistable modulation," Nat. Methods **9**(12), 1171–1179 (2012).
34. E. Y. S. Yew, C. J. R. Sheppard, and P. T. C. So, "Temporally focused wide-field two-photon microscopy: Paraxial to vectorial," Opt. Express **21**(10), 12951–12963 (2013).
35. F. Duck, *Physical Properties of Tissue: A Comprehensive Reference Network* (Academic Press, 1990).
36. E. Tal and Y. Silberberg, "Transformation from an ultrashort pulse to a spatiotemporal speckle by a thin scattering surface," Opt. Lett. **31**(23), 3529–3531 (2006).
37. J. Mattis, K. M. Tye, E. A. Ferenczi, C. Ramakrishnan, D. J. O'Shea, R. Prakash, L. A. Gunaydin, M. Hyun, L. E. Fenno, V. Gradinaru, O. Yizhar, and K. Deisseroth, "Principles for applying optogenetic tools derived from direct comparative analysis of microbial opsins," Nat. Methods **9**(2), 159–172 (2011).
38. A. M. Packer, D. S. Peterka, J. J. Hirtz, R. Prakash, K. Deisseroth, and R. Yuste, "Two-photon optogenetics of dendritic spines and neural circuits," Nat. Methods **9**(12), 1202–1205 (2012).

1. Introduction

With the advent of computer generated holography (CGH), arbitrary optical excitation patterns are generated routinely by now for many applications, including optical trapping, photostimulation, and optical lithography [1–4].

In CGH, excitation patterns are formed by placing a spatial light modulator at the Fourier conjugate plane to the imaging plane, and applying an appropriate phase mask to obtain an excitation intensity pattern as close as possible to the desired one. The required phase mask is

usually found via an iterative method [5,6]. For optical trapping or multisite uncaging, 2D and 3D holographic generation of near-diffraction-limited spots [4,7–10] have been used. For applications in photostimulation or lithography the use of holographic extended pattern is preferred as it permits to quickly cover large excitation areas [3,11]. When combined with temporal focusing (TF), this can also be achieved with micrometric axial resolution [11,12].

CGH is usually applied under conditions when the excited sample is either transparent or weakly scattering, while little is known on the use of this approach within a scattering specimen.

For improving the quality of diffraction-limited spots after propagation in scattering media, the preferred approach is adaptive optics (AO) [13–16], which is technically compatible with CGH [17–19]. In addition to the beam modulation required to generate the excitation pattern, an extra correction is applied to the beam to pre-compensate for distortion induced by sample scattering or optical aberrations of the system. The main difficulty with AO based approaches is the time consuming adaptive optimization process, through which the required correction for precompensation is found. Moreover little data has been reported for the use of AO to improve the quality of extended holographic patterns [19].

An alternative to AO is the use of robust excitation beams, which possess inherent resilience to scattering, such as Bessel beams. 'Bessel beams' [20] reconstruct their original shape regardless of the particular realization of scattering inside the medium and have recently been used for a variety of applications, including particle trapping [21] and light-sheet microscopy [22]. However, a major disadvantage of these non-diffracting beams, in the context of photostimulation, is the complete absence of optical sectioning and that the excitation shape is limited to a circular geometry.

We have recently shown that, alternatively to AO or Bessel beams, efficient in-depth generation of extended patterns can be reached by combining TF either with low-numerical aperture (NA) Gaussian beams or beams generated with generalized phase contrast (GPC) [23,24]. This permits generation of excitation patterns with some degree of resilience to scattering, due to the reduced degree of correlation between speckle patterns imprinted on the various color components of the excitation pulse, which traverse the sample at different directions. We could demonstrate the propagation of temporally focused shaped patterns deep in scattering medium with almost no distortion of the shape and reasonably good optical sectioning even at depths reaching 2-3 scattering lengths and show the applicability of this method to activate neurons expressing channelrhodopsin-2 (ChR2), the most used optogenetic channel, in-depth [25]. The self-healing effects of TF in scattering media were also discussed recently in a work showing the robustness to scattering of line TF over widefield TF [26].

Here, we extend our previous investigation to the propagation of shaped holographic beams with and without TF, through fixed and acute brain slices. We show that CGH generated patterns are very robust to scattering (in the sense of preservation of the excitation shape), and that the combination with TF enhances axial confinement up to several scattering lengths deep into the excited sample. This permits efficient excitation of cortical neurons expressing the red-shifted opsin C1V1 [27]. This is the first demonstration of extended holographic patterns in two-photon excitation used to activate an optogenetic actuator. Our findings may also be of relevance in performing deep-tissue imaging via the use of temporally focused structured light [28,29].

2. Methods

2.1 CGH-generated beam illumination

In the experimental setup the laser beam from a Ti:Sapphire oscillator (MaiTai, Spectra-Physics) was expanded (10x) in order to match the input window of a Liquid Crystal on Silicon Spatial Light Modulator (LCOS-SLM) (Hamamatsu Photonics X10468-02 or −07), illuminated at oblique incidence, as in previous works [11,12]. The beam's wavefront at the SLM plane was modified by using a custom-designed software [2] that calculates the

corresponding phase-hologram by using the iterative algorithm. The beam reflected from the LCOS-SLM was Fourier transformed by a 1000 mm focal length achromatic lens and formed a first image of the target intensity onto the grating for TF or a mirror if TF was not used. A 500 mm focal length achromatic lens completed the optical setup so that the SLM plane was conjugated with the back focal plane of the microscope objective. In this way a depth-resolved temporally focused excitation pattern was generated at the focal plane of the objective, whose lateral spatial distribution was a reduced (~1/170) replica of the pattern generated on the grating. After entering the microscope (Olympus BX50WI), the laser beam was reflected by a dichroic mirror (Chroma Technology 640DCSPXR) before propagating through the objective. Fluorescence was filtered by a HQ535/50M emission filter (Chroma Technology) then collected by a CCD camera (CoolSNAP HQ2, Roper Scientific). To measure the axial propagations (y-z profiles), we used a configuration with two opposite placed objectives, as the one described in [11].

2.2 Quantification of transmitted image quality

To characterize pattern uniformity, P, we compute the intensity cross-correlation within a region of interest, A, containing the excitation shape:

$$P = \iint_{dA} I_d\left(x,y\right) I_s\left(x,y\right) \Big/ \sqrt{\iint_{dA} I_d\left(x,y\right)^2 \iint_{dA} I_s\left(x,y\right)^2} , \qquad (1)$$

where I_d is the desired intensity pattern (without scattering) and I_s is the measured (simulated) one. For no distortion $P = 1$.

CGH patterns are speckled patterns. Upon propagation the patterns maintain their overall shape but change the particular speckle distribution within this shape. Since we are interested in a measure of pattern distortion due to scattering, we convolved both I_d and I_s with a Gaussian filter with the width of the CGH speckles. The pattern uniformity, P, was calculated for the Gaussian filtered patterns, thus disregarding the particular small speckle distribution.

2.3 Preparation of fixed slices

Sprague Dawley rats from postnatal days 19 to 30 were perfused transcardially with a 4% paraformaldehyde solution in a 0.1 M phosphate buffered saline (PBS). Brains were extracted and postfixed overnight at 4°C. Coronal cortical slices from 50 to 250 μm were obtained on a Leica VT1000 slicer and kept in PBS containing sodium azide (0.01%) at 4°C. Slices were observed in the optical setup in a PBS solution.

We performed our study by always illuminating the same area of the cortex (layer II-III or layer IV), in order to be consistent for all measurements and not to have extra variations of the results, caused by the heterogeneity of different brain regions.

2.4 Preparation of acute rat cortical slices

Coronal cortical slices (250 to 550 μm) were obtained on a Leica VT1200S slicer from postanatal rats (between 21 and 28 days) in an ice-cold slicing solution containing (in mM): 125 NaCl, 1.25 KCl, 1 CaCl$_2$, 1.5 MgCl$_2$, 1.25 KH$_2$PO$_4$, 25 NaHCO$_3$ and 16 Glucose. The slices were incubated in a chamber containing the same solution at 33°C for 30 minutes and then left at room temperature. Those solutions were oxygenated (95% O$_2$, 5% CO$_2$) during the whole experiment. Slices were observed in the double microscope configuration in a HEPES based solution containing (in mM): 132 NaCl, 4 KCl, 1 MgCl$_2$, 2.5 CaCl$_2$, 2NaHCO$_3$, 10 HEPES, 25 Glucose (pH 7.3).

2.5 Cortical C1V1$_{TT}$ expression

Mice (4-weeks old) were put in deep anesthesia with intraperitoneal injection of ketamine (80 μg/g body weight; Ketamine 1000, Virbac France) and xylazine (10 μg/g body weight;

Xylazine Rompun 2%, Bayer Healthcare) and mounted in a stereotaxic frame. A midline sagittal incision was made to expose the cranium over the cortex. At the site of injection (1 mm posterior and 1.5 mm lateral to Bregma) a 1 mm^2 burr hole was drilled and a 36-gauge stainless steel beveled needle (Coopers Needleworks Ltd.) was slowly descended 0.5 mm through a small slit cut in the meninges. After a 2-min pause, the needle was retracted 100 μm and then 1.5 μL (6,705·10^9 total genome copies) of AAV2/9.CaMKIIα-C1V1(E122T/E162T)-TS-eYFP-WPRE-hGH (University of Pennsylvania vector core) were injected at a rate of 0.1 μL/min. Once completed, the needle was left in place an additional 5 min before being withdrawn, and the scalp was closed with cyanoacrylate (Henkel). Finally, the mouse was injected peritoneally with antisedan (0.2 μg/g, Janssen) and subcutaneously with 0.3 ml warm 0.9% saline solution to allow for quick recovery from the anesthesia. The mouse was kept under a warming lamp until fully recovered before finally being returned to standard housing. Viral expression lasted 8 weeks.

2.6 Preparation of acute mice cortical slices and electrophysiology

Coronal cortical slices (300 μm) were obtained on a Leica VT1200S slicer from injected mice (2-3 months old) in an ice-cold slicing solution containing (in mM): 230 Sucrose, 3 KCl, 0.8 CaCl$_2$, 8 MgCl$_2$, 1.25 NaH$_2$PO$_4$ and 26 NaHCO$_3$. (2R)-amino-5-phosphonovaleric acid (AP5, Abcam) 50 μM was added to the slicing solution. Electrophysiology was performed in slices in an extracellular solution containing (in mM): 125 NaCl, 3 KCl, 1 MgCl$_2$, 2 CaCl$_2$, 26 NaHCO$_3$, 1.25 NaH$_2$PO$_4$, 25 Glucose (pH 7.3). The slices were incubated in a chamber containing the same solution at 33°C for 30 minutes and then left at room temperature. Those solutions were oxygenated (95% O$_2$, 5% CO$_2$) during the whole experiment. Neurons were identified visually under an upright fluorescence microscope with DIC illumination (Olympus BX51). Patch pipettes (4-7 MΩ) were used to record whole cell currents with an Axon 200B amplifier, filtered at 4 kHz, and digitized at 10 kHz using a digidata board and Clampex software (Axon Instruments). Intracellular solution was adapted from Gasparini et al. [30] and contained (mM): 120 KMeSO$_4$, 20 KCl, 10 HEPES, 0.5 EGTA, 4 NaCl, 4 K$_2$ATP, 0.3 Na$_2$GTP, 14 phosphocreatine (pH 7.25).

All reagents were purchased from Sigma Aldrich unless stated otherwise.

3. Results

We evaluated the propagation of holographic generated beams with and without TF, with numerical simulations (Fig. 1) and experimentally (Fig. 2). We found in both that, up to a scattering sample of 250 μm thickness, spot shapes generated with CGH were quite robust against scattering even without TF (x-y and y-z cross sections in Fig. 2(A)). Indeed, the pattern uniformity calculated for smoothed patterns (where speckles are smoothed by convolution with a Gaussian filter, see Methods), both with and without TF was about 0.95, in agreement with the simulation results of Fig. 1. The normalized axial intensity profiles for the y-z cross section of Fig. 2(A) are shown in Fig. 2(B).

The axial light distribution for different slice thicknesses for CGH and TF-CGH beams is shown in Fig. 2(C). As already found in the case of TF-GPC beams [25], axial confinement was well maintained at depths reaching the scattering length (135 μm for these samples [25]) for both CGH and TF-CGH and started deteriorating at greater depths. Although this deterioration is more significant for TF-CGH beams than for CGH beams alone, axial resolution of TF-CGH beams remained better than that of CGH.
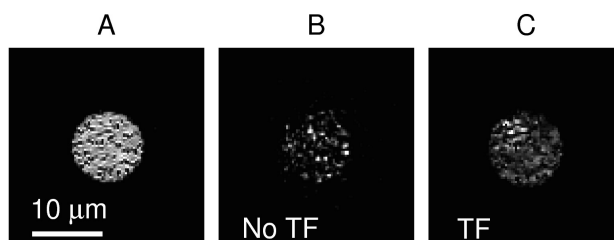
Fig. 1. Multiphoton excitation pattern generated at the focal plane of the objective by numerical simulation of the propagation of a holographic beam generating a spot of 10 µm, through 200 µm of a turbid medium consisting of 2 µm dielectric spheres randomly distributed, having a refractive index higher by 0.1 than the surrounding medium and an average concentration of 1 sphere per 1000 µm³. This gives rise to a scattering length of ~135 µm, similar to that typically observed in brain tissue [25,31]. The image of the holographic spot (A) not scattered, (B) scattered but not temporally focused and (C) scattered and temporally focused are illustrated. Simulations were performed at 800 nm, with 100 fs laser pulses. The pattern uniformity was about 0.96 for the temporally focused pattern and 0.92 for the non-temporally focused one.

In order to characterize the maximal depth at which patterned photostimulation can be employed in live tissue, we tested the propagation of holographic patterns through acute cortical brain slices (300-550 µm thick) prepared from juvenile rats. As in the experiments with fixed slices, we studied the effects of scattering on the excitation shape and axial resolution by recording the images on a thin fluorescent layer after propagation through brain slices of different thicknesses. For these experiments, we used a longer excitation wavelength of 950 nm that should mitigate the effects of scattering and excites less autofluorescence from the tissue surface.

In Fig. 3(A), we show the effect of scattering on the transmitted shape of a holographic beam generating a 15 µm spot at the objective focal plane with and without TF. In agreement with the results obtained for fixed slices, the shapes of CGH beams appeared extremely robust to scattering. TF-CGH transmitted shapes exhibited almost no distortion even after 550 µm, while for CGH without TF, the original shape started to be affected at around 300 µm. The pattern uniformity as defined in Methods was 0.95 up to a depth of 550 µm for TF-CGH, but decreased to about 0.85 in the absence of TF at the same depth.

y-z cross sections are also shown in Fig. 3(A) (lower panels). The tilt in the y-z cross section observed as the beam propagated through slices over 300 µm thick was similar to the one observed in other works studying diffraction-limited spot propagation through tissue and could be attributed to refractive index mismatch at the sloping surface of the slice [32]. The average FWHM values measured for temporally focused holographic spots after propagation through the tissue (6 different realizations in the cortex area, layer II-III or IV, as in the case of fixed slices) are shown in Fig. 3(B). Similarly to what has been reported for the case of GPC-TF [25], here we found that the axial resolution starts to deteriorate after propagation through depths greater than one scattering length. At 550 µm, the axial response widened by a factor of approximately 3 times larger than what is achievable in absence of scattering. Even under these conditions, however, the measured axial resolution (~12 µm), should enable photoactivation with nearly single cell precision.

After demonstrating the robustness of CGH shaped patterns against scattering, we next verified the efficiency of TF-CGH beams in photoactivation of neurons. In order to demonstrate that, we performed whole-cell patch clamp of neurons expressing the red-shifted chimeric opsin C1V1 [27] in cortical brain slices. C1V1 was excited at 1040 nm as in [33]. We first measured the average current generated by a 15 µm diameter holographic spot placed on the cell soma (267 ± 85 pA at 0.5 mW/µm² after the objective, 50 ms illumination duration, n = 6 cells, Fig. 4(A)), before switching to current clamp mode in order to record action potentials (APs). Depending on the expression level of the channel and the intrinsic properties of neurons, we managed to trigger single APs with pulses as short as 1 ms and

delivering 0.5 mW/μm^2 after the microscope objective (Fig. 4(B), 2 out of 6 cells). To trigger APs reliably independent of expression levels, the pulse duration had to be set at 10 ms. We finally tried to generate AP trains up to 10 Hz (1-10 ms pulses every 100 ms at 0.5 mW/μm^2, Fig. 4(C)). This protocol was successful in the 2 neurons that had the highest expression level (and therefore the largest currents for 50 ms light pulses) out of 5 cells.
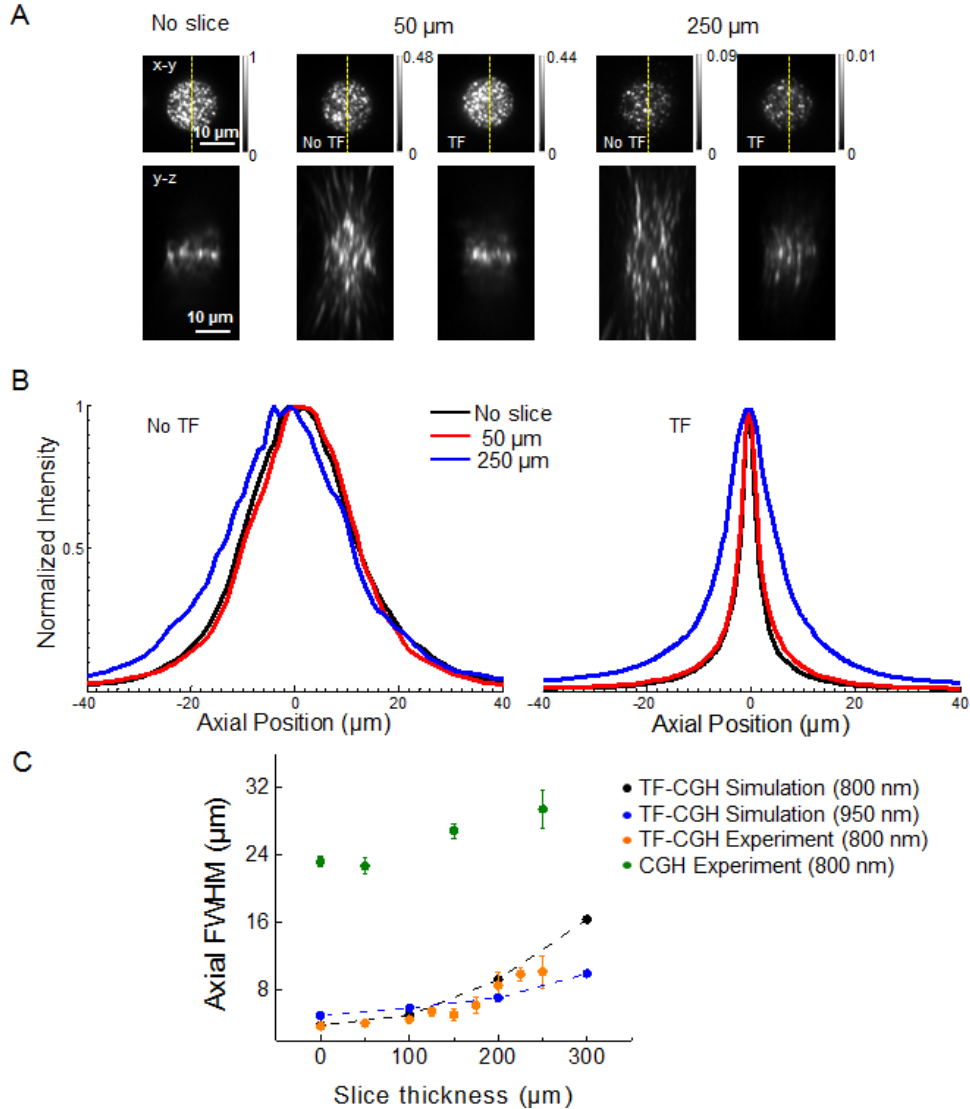

Fig. 2. (A) Top: x-y cross sections of the holographic beam at the objective focal plane, without scattering tissue and after propagating through 50 and 250 μm fixed brain slices, with or without TF in the optical setup; Bottom: corresponding y-z cross sections along the yellow dashed lines. λ = 800 nm. (B) Normalized axial intensity of the y-z cross sections shown in (A) without and with TF implementation. In the absence of scattering the temporally focused cross section is shown. (C) Variation of the FWHM of the axial intensity distribution of the holographic spot in A, in respect to the scattering depth. Black and blue dots correspond to theoretical modeling at 800 and 950 nm respectively for TF-CGH, orange dots correspond to experimental data for TF-CGH, and green dots correspond to experimental data for CGH beams alone. Experimental data is given as average ± STD values from 4 different realizations for each thickness. The gray-scale level in (A) is normalized to the peak intensity of the fluorescence image without scattering.
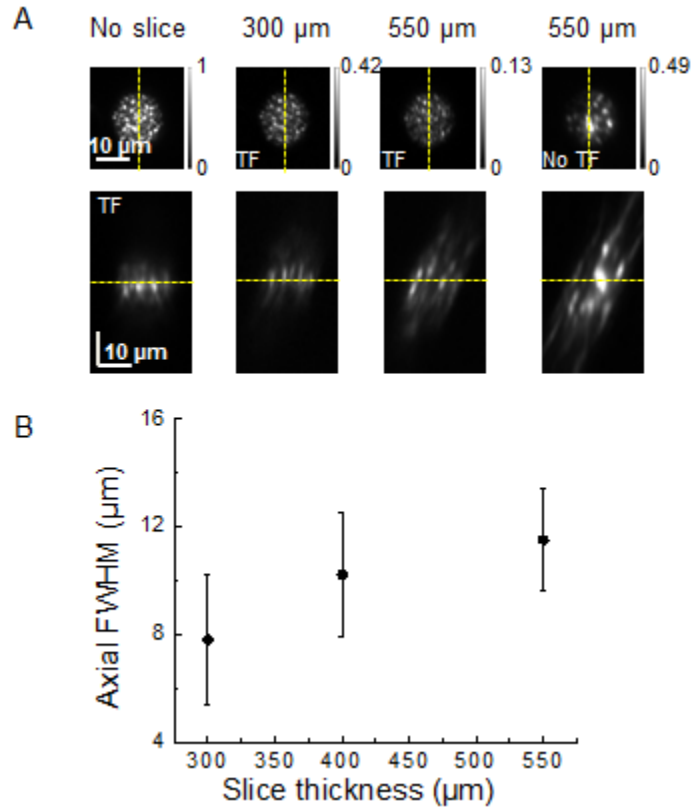
Fig. 3. (A) x-y and y-z 2P fluorescence cross sections of a 15 μm holographic spot. From left to right: without scattering, after propagation through acute cortical brain slices of 300 μm with TF, 550 μm with TF and 550 μm without TF in the optical setup. (B) Variation of the FWHM of the axial intensity distribution of the temporally focused holographic spot in respect to the scattering depth. Data corresponds to average ± STD values from 6 different realizations for each thickness. λ = 950 nm. The gray-scale level is normalized to the peak intensity of the fluorescence image without scattering.
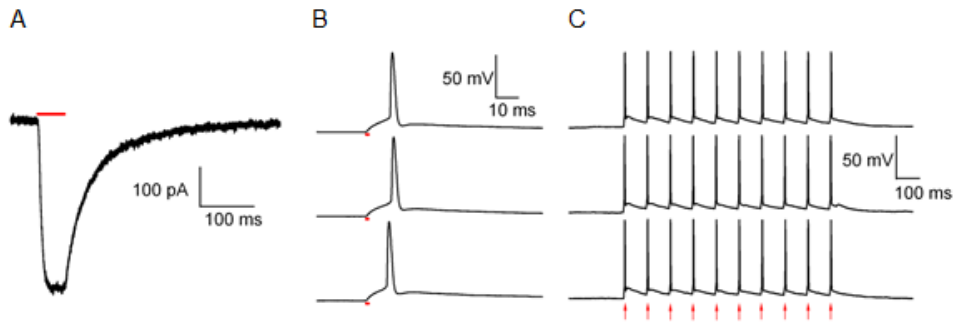
Fig. 4. Holographic activation of C1V1$_{TT}$. (A) Representative whole cell current recorded during a 50 ms pulse at a power of 0.5 mW/μm^2. (B) Single action potentials could be reliably triggered in cells expressing C1V1$_{TT}$. Here is one example with 1 ms pulses at 0.5 mW/μm^2. (C) Example of 10 Hz trains generated with a holographic spot (2 ms pulses every 100 ms, 0.5 mW/μm^2). For all panels: λ = 1040 nm, spot diameter 15 μm. Laser power is given after the objective.

4. Discussion

We investigated theoretically and experimentally the propagation through both fixed and acute brain slices of extended patterns generated by holographic beams. For the theoretical simulation, we used the same numerical model as in [25] based on Fresnel propagation in a scattering phantom that reproduced biological tissue properties, but have verified that vectorial effects [34] are not significant under the experimental conditions used here.

The presented data exhibits two separate but related phenomena. The first is that even without temporal focusing, the transverse shape of CGH beams exhibit significant resilience to scattering. The second is the increased depth of penetration when combining CGH with TF. Let us first discuss the origin of the former.

As can be seen in Fig. 2, CGH beams (without TF) exhibit robustness to scattering in the sense that the pattern overall shape and the axial confinement are maintained to a good extent, even at depths corresponding to 1-2 scattering lengths, λ_s. This is in stark contrast with observations on low-NA Gaussian beams or shaped beams generated with GPC [25], where significant shape distortion is already observed at depth of the order of the λ_s. The origin of this difference lies within a combination of the scattering medium properties and the angular spectrum content of the CGH excitation beam.

The scattering medium of interest (i.e. brain tissue) is a predominantly forward-scattering medium, scattering light at small angles [35]. In the spatial frequency domain, this means that scattering events correspond to small changes in the spatial frequency content. The propagation of light through the scattering medium can thus be viewed as a diffusion process in the spatial frequency domain, mixing between nearby spatial frequency components. Each scattering event results in a small spatial frequency shift, and the probability for each frequency component to deviate considerably from its initial value grows with the scattering medium thickness. High spatial frequencies – corresponding to large angles – propagate a longer path in the scattering medium. They thus have a higher probability to deviate more significantly from their initial value than lower spatial frequencies. In other words, higher spatial frequencies will be scattered to lower frequencies with higher probability than vice versa. The initial spatial frequency content of CGH beams is broad, ranging from a forward propagating (DC) term, all the way up to the numerical aperture of the excitation objective. Within this broad envelope, there is a low correlation of the phase among neighboring spatial frequencies. This is the origin of diffraction-limited speckles in the image plane.

Considering the small angle scattering discussed above, to a first approximation, CGH beam propagation in brain tissue merely results in energy reshuffling among nearby spatial frequencies. Thus, the phase structure in spatial frequency domain is altered, but the envelope is not significantly modified. This, in turn, modifies the details of the speckle pattern but maintains the overall shape. As an additional result, the axial confinement is also maintained. In contrast, low-NA Gaussian or GPC beams are mostly centered on the DC spatial frequency term, and their spatial frequency content is strongly altered by scattering, leading to the formation of large and non-uniform speckles after propagating through brain slices.

For propagation of CGH beams in thicker brain slices, the scattering of high frequencies to lower ones becomes more dominant. Therefore, low frequency content becomes significant, and scattering effects reveal themselves in the appearance of larger speckles (smaller spatial frequencies) and deterioration of the axial confinement, as is evident in the experimental data presented in Fig. 3.

When TF is introduced, the robustness to scattering of the CGH beams increases. This is due to the fact that with TF the ballistic photons contribute a much more significant fraction of the total excitation signal. When TF beams propagate through a scattering medium, different colors propagate through different paths [25]. As a result, the phases of scattered photons of different colors are mostly uncorrelated whereas those of the ballistic photons are correlated. The ballistic photons, having correlated phases, arrive at the focal plane as a short pulse, whereas scattered photons lead to temporal speckle, distributing the energy over a longer temporal window [16,36]. Due to the dependence of the two-photon absorption

process on the inverse of the pulse duration this leads to an accentuation of the ballistic photon signal.

To support the above explanation we performed analysis of the frequency content of experimentally measured images. Figure 5 depicts the reduced migration of high frequencies to lower ones of TF-CGH beams in comparison to CGH beams due to scattering. The figure shows the frequency content of 3 pairs of images, TF-CGH and CGH beams, for brain slices of thicknesses 300, 400 and 550 μm. For the 300 μm slices the spatial frequency content of the TF-CGH and CGH beams is roughly similar. However, as the scattering medium becomes thicker, the TF-CGH beam frequency content remains more or less constant while for the CGH beam the relative contribution of low spatial frequencies increases while that of the high spatial frequencies decreases.
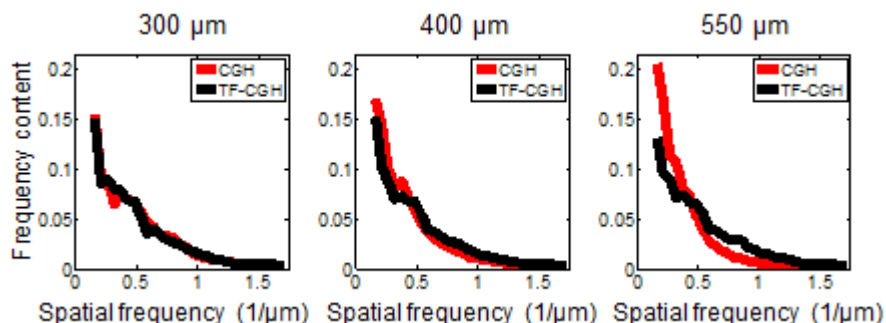

Fig. 5. Frequency content of CGH vs. TF-CGH beams after scattering through brain slices of thickness 300, 400 and 550 μm. The frequency content is the fraction of energy in a given frequency.

This can be alternatively viewed in a time domain picture. TF performs an ultrafast line scanning of the image plane, while for non-TF CGH the entire image is illuminated simultaneously. Thus, without TF, scattered photons interfere with the ballistic ones throughout the entire illuminated region. In contrast, with TF, only a thin line is illuminated at each moment, and in order to interfere with the ballistic photons, scattered photons have to scatter onto it, which is an event with a much lower probability. This is illustrated in Fig. 6. For TF-CGH beams this results in an increase of the scattering medium thickness before scattering effects become apparent. This time domain picture also illuminates the similarity between the dependence of the axial resolution of TF-CGH beams on the scattering medium thickness, as shown in Fig. 2(C), and that observed with TF-GPC [25].

Finally, we demonstrated that TF-CGH beams can efficiently photoactivate the red-shifted opsin C1V1 [27] expressed in cortical neurons. C1V1 is a new red variant of excitatory opsins exhibiting a longer closing time (~50 ms) and a red shifted absorption spectrum [37]. The longer closing time facilitates its use with scanning approaches enabling a more efficient summation of currents generated at the beginning of the scan with those generated at the end. Indeed, single cell AP generation in brain slices [33,38] and *in vivo* [38] has been recently demonstrated by using C1V1 and laser scanning photoactivation.

Here, we demonstrated that using TF-CGH enables reaching a temporal resolution for single AP generation of 1 ms, that is 5 to 70 times shorter than what has been reported with scanning approaches. In contrast to scanning approaches that could reach spiking frequency of 20 Hz reliably [33] and to what we demonstrated when photoactivating ChR2 with TF shaped beams [24], we could not evoke spiking frequency higher than 10 Hz probably due to the long closing time of C1V1 and the maximum laser power at our disposal. Nonetheless, using 1040 nm as the excitation wavelength, we could reliably trigger single APs with a fraction of the available power of our laser. Holographic beams split power over the illuminated area of all patterns, so theoretically, considering the available laser power from a Ti:Sapphire oscillator, up to 4 cells could have been excited at the same time in our

conditions. Recent laser sources at 1064 nm can generate 8 times more power [38], thus possibly enabling at this depth the simultaneous activation of approximately 30 cells.
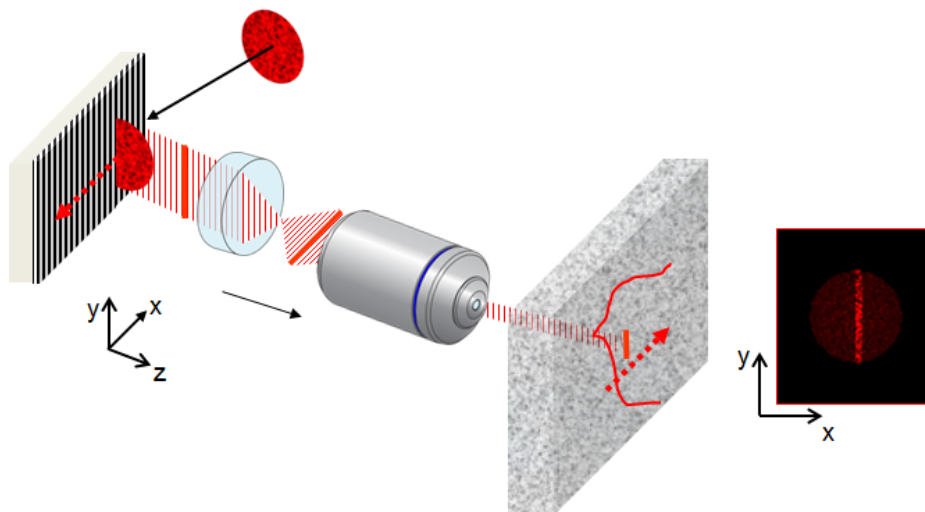

Fig. 6. The propagation of a large beam diffracted by the grating produces an ultrafast line scanning of the sample (inset). Scattering events off the scanning line at a single moment in time cannot interfere with the ballistic photon in the line.

Acknowledgments